Optimization of a Piezoelectric Energy Harvester for Small Scale Applications

R. S. Diogo∗

Instituto Superior Técnico, Universidade de Lisboa, Av. Rovisco Pais, 1049-001 Lisbon, Portugal

∗ruidiogo@tecnico.ulisboa.pt

May, 2016

Abstract: For the past decade, piezoelectric energy harvesting has come a long way from being an unreliable power source, often associated with low power outputs. Progressive technological advances have allowed energy harvesters to improve significantly, becoming more efficient and cost effective, thus making them a serious and promising solution for the future of global power demand. The main focus of this thesis concerns the material and structural optimization of a circular plate energy harvesting device. This plate is analyzed in an open circuit, in order to maximize the absolute value of the output electrical potential, via optimization. To this end, a computational optimization model was developed in Matlab, using a structural finite element (FE) model defined in Abaqus to perform a static analysis of the performance of the harvester. This computational model involves the programming of the necessary scripts to allow the automatic communication of the Matlab code and Abaqus program, in order to accommodate the iterative nature of the optimization problem. Two distinct optimization algorithms were tested: Simulated Annealing and Pattern Search, both included in the standard Matlab toolbox. Furthermore, two separate case studies were carried out, concerning the modelling of the piezoelectric material. The material structure was modelled both as a single crystal and as a polycrystal. In the former case, the design variables concern the single crystal orientation and also a geometry parameter. For the polycrystalline case, probabilistic variables were introduced in the optimization model and an additional finite element code for the asymptotic homogenization of the polycrystal was used.

1. Introduction

Simply put, *piezoelectricity* is the electric charge that builds up in some materials, such as certain crystals, ceramics and polymers, as a response to an experienced stress state. The *piezoelectric effect*, in turn, can be defined as a linear electromechanical interaction. In the direct effect, applied pressure generates electricity, while in the converse effect, pressure is generated from an externally applied voltage [1]:

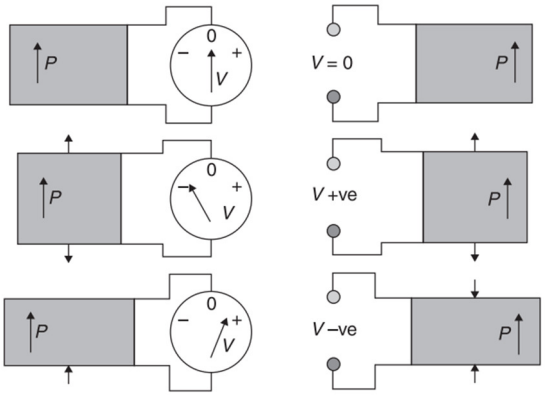

Figure 1 – The direct (a) and converse (b) piezoelectric effect[1].

The concept of *energy harvesting* or *scavenging* pertains to the extraction of small amounts of energy from the ambient environment through various sources of energy. The available energy for harvesting is mainly provided by ambient light and radio frequency, as well as thermal (heat) and mechanical (forces, pressure and vibrations) sources [2].

Most promising applications for *PEHs* (*Piezoelectric Energy Harvesters*) are still in their developing stage, although some models are already commercially available. There is still much debate regarding the efficiency and performance that can be expected from this technology in the upcoming years. Nonetheless, PEH devices have attracted wide attention from researchers, especially in the last decade, due to their prominent advantages, such as high power density, architectural simplicity and scalability. As a result, the number of studies on piezoelectric energy harvesting published in recent years is more than twice the sum of publications on its electromagnetic and electrostatic counterparts [3]:

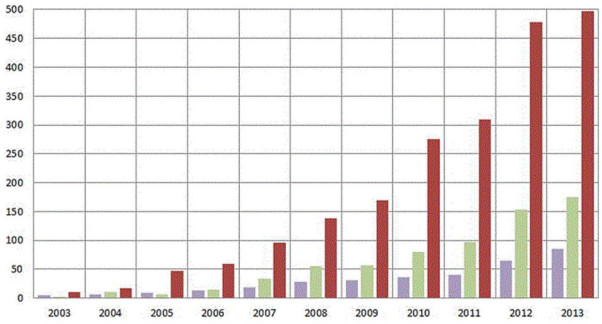

Figure 2 – Number of published papers on piezoelectric (red), electromagnetic (green) and electrostatic (purple) energy harvesting on the *Web of Science* website, from 2003 to 2013[2].

This technology's state of the art can be divided into four distinct categories, according to the devices' diminishing dimensions: macro and mesoscale, two classes that are often grouped due to their lax definition, but meaning essentially

[1] From: Cochran, S., Nakamura, K. (2012), *Ultrasonic transducers*, Woodhead Publishing.

[2] From: Toprak, A., Tigli, O. (2014), *Piezoelectric energy harvesting: State-of-the-art and challenges,* Applied Physics Reviews 1-031104, AIP Publishing.

that they can be manually assemblable; microscale (also known as the MEMS scale), in which the recurrence to standardized photolithography techniques is present, and nanoscale, where the production of devices is made possible by the use of piezoelectric nanofibers. The size of a PEH affects various parameters such as its weight, fabrication method, achievable power output level and potential application areas. In this work, the analyzed diaphragm (a thin plate) can be classified as a MEMS-type device, due to its characteristic dimensions.

The circular plate configuration for a PEH was first proposed by Umeda *et al.* in 1996 as a means of converting the kinetic energy from an impact into consumable electrical energy. Since then, other works have been published on this particular setup, such as the ones from Horowitz *et al.* (2006) and Khuene *et al.* (2008). However, in 2003, Kim *et al.* published a paper in which they investigated the possibility of harvesting pressure derived energy from a thin disk PEH. Their study of the stress distribution throughout the circular plate, under an encastre boundary condition, led to the suggestion of a new layout regarding material polarization. This is the starting point for the layout considered in this thesis. It consists of two concentric circular piezoelectric layers and a subjacent metallic substrate layer.

There are an exceedingly abundant number of relevant and currently applicable examples of piezoelectric energy harvesting technologies to mention every single one of them. We are currently living in a possible turning point in the global energy production history, and while PEH applications are currently still number two to energy solutions that harvest thermal or electromagnetic sources, these same preferred technologies are known for their wanting reliability and consistency, regarding power output volume.

2. Governing Equations, FE Problem Formulation and Homogenization

The linear theory for piezoelectricity assumes that both the displacement gradient and electric field (electric potential gradient) are infinitesimal, in the sense that [4]:

$$\left|u_{i,K}\right| \ll 1, \quad \left|E_i = \frac{\partial \phi}{\partial x_i}\right| \ll 1 \tag{1}$$

For an infinite continuous piezoelectric medium, the piezoelectric constitutive relations are as follows [5]:

$$T_{ij} = c^E_{ijkl} S_{kl} - e_{kij} E_k \tag{2}$$

$$D_i = e_{ikl} S_{kl} + \varepsilon^S_{ik} E_k \tag{3}$$

where T_{ij}, c^E_{ijkl}, S_{kl}, e_{kij} and ε^S_{ik} are the stress, elastic, strain, piezoelectric constants (stress form) and electric permittivity tensors, respectively. E_k and D_i represent the electric field and electric displacement vectors, respectively.

As for the finite element model, these are the differential equations that translate the problem's definition, along with (2) and (3):

$$T_{ji,j} = \rho \ddot{u}_i \tag{4}$$

$$S_{ij} = \frac{u_{i,j} + u_{j,i}}{2} \tag{5}$$

$$D_{i,i} = 0 \tag{6}$$

$$E_i = -\phi_{,i} \tag{7}$$

These expressions correspond to the motion equation, the strain-displacement relation, charge equation and the electric field-potential relation, in order. However, this system can only be solved when boundary conditions are defined:

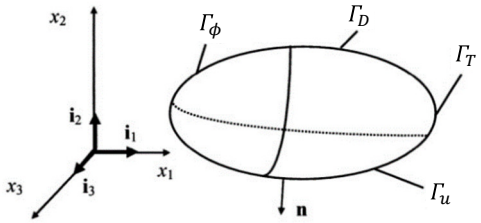

Figure 3 – A generic piezoelectric body's surface partition, where $\boldsymbol{n}$ is the normal unit vector for the surface Γ [3].

The S surface's partitions that delimitate the generic piezoelectric body volume V are assumed as follows:

$$\Gamma_u \cup \Gamma_T = \Gamma_\phi \cup \Gamma_D = \Gamma, \quad \Gamma_u \cap \Gamma_T = \Gamma_\phi \cap \Gamma_D = \emptyset \tag{8}$$

where Γ_u and Γ_T symbolize the partitions with a prescribed displacement and load, respectively. Similarly, Γ_ϕ represents the part of Γ where an electrode condition is imposed, i.e., a region where the electric potential is exclusively time-dependent, whereas Γ_D corresponds to the zone where this condition is absent. On this unelectroded part of Γ, the charge condition can be written as:

$$D_j n_j = 0 \tag{9}$$

The work carried out in this thesis also concerns the homogenization of the piezoelectric material properties, for the polycrystal. To this end, the asymptotic homogenization theory for piezoelectricity, initially developed by Telega in 1990, was implemented through an additional finite element code. This theory rests on the assumption that the material is formed by the periodic repetition of a small microstructural representative volume element (RVE). The final properties are given by the three following expressions[4] [7,8,9]:

$$c^h_{rspq}(\mathbf{x}) = \frac{1}{|Y|}\int_Y \left[c_{ijkl}(\mathbf{x},\mathbf{y}) \left(\delta_{ip}\delta_{jq} + \frac{\partial \chi_i^{(pq)}}{\partial y_j} \right) \times \left(\delta_{kr}\delta_{ls} + \frac{\partial \chi_k^{(rs)}}{\partial y_l} \right) + e_{kij}(\mathbf{x},\mathbf{y}) \left(\delta_{ip}\delta_{jq} + \frac{\partial \chi_i^{(pq)}}{\partial y_j} \right) \frac{\partial \psi^{(rs)}}{\partial y_k} \right] \mathrm{dY} \tag{10}$$

[3] Adapted from: Yang, J. (2005), *An Introduction to the Theory of Piezoelectricity,* Springer.

[4] The notation used in these expressions is compliant with [6].

$$e^h_{prs}(\mathbf{x}) = \frac{1}{|Y|}\int_Y \left[e_{kij}(\mathbf{x},\mathbf{y})\left(\delta_{kp} + \frac{\partial R^{(p)}}{\partial y_k}\right)\left(\delta_{ir}\delta_{js} + \frac{\partial \chi_i^{(rs)}}{\partial y_j}\right) - e_{kij}(\mathbf{x},\mathbf{y})\frac{\partial \Phi_i^{(p)}}{\partial y_j}\frac{\partial \psi^{(rs)}}{\partial y_k}\right] \mathrm{dY} \quad (11)$$

$$\varepsilon^h_{pq}(\mathbf{x}) = \frac{1}{|Y|}\int_Y \left[\varepsilon_{ij}(\mathbf{x},\mathbf{y})\left(\delta_{ip} + \frac{\partial R^{(p)}}{\partial y_i}\right)\left(\delta_{jq} + \frac{\partial R^{(q)}}{\partial y_j}\right) - e_{kij}(\mathbf{x},\mathbf{y})\left(\delta_{jq} + \frac{\partial R^{(q)}}{\partial y_k}\right)\frac{\partial \Phi_i^{(q)}}{\partial y_j}\right] \mathrm{dY} \quad (12)$$

$\chi_i^{(rs)}$ and $R^{(p)}$ indicate the characteristic displacement and electric potential of the unit cell Y; $\psi^{(rs)}$ and $\Phi_i^{(p)}$ are characteristic coupling functions. Although these equations have an analytical solution for simpler cases, such as the one-dimensional unit cell case, more complex RVEs require the use of the FE method for a solution to be found (see [6]).

3. Optimization

The ultimate goal of this thesis concerns the maximization of the absolute value of the piezoelectric harvester's electric potential output, in an open circuit configuration. The main tools that make this objective possible are called optimization algorithms. Two optimizers were tested: Simulated Annealing, a stochastic approach which emulates the crystallization process that occurs during metal cooling and Pattern Search, an algorithm that can perform a smart, multi-directional search for an optimum solution in a constrained domain [10]. Setting up the global optimization problem translates to defining the design variables and their value constraints, as well as an objective function that can be evaluated in an iterative fashion.

The design variables depend on the material case (single or polycrystal) being considered. Nevertheless, in both cases there are variables that concern the material's polarization, as well as an additional geometric variable. The polarization variables relate to the orientation in which the piezoelectric ceramic material has been poled. Ultimately, they control the principal axis of polarization, which in turn dictates how each zone of the plate develops piezoelectricity in response to the applied pressure.

For the single crystal case, these orientations are defined by three Euler angles: ϕ, θ and ψ. The polarization of the piezoelectric medium is implemented through the creation of a user-defined coordinate system, in Abaqus, for each region. The polycrystalline model, however, requires an additional standard deviation-related variable per piezoelectric region, since, in this case, probabilistic distributions of polarization are considered for the material; the three aforementioned angles still exist for each zone, only now they represent a mean value, necessary for the definition of a distribution. These angle distributions are then fed to the homogenization program, which in turn can now compute the homogenized material properties. The properties are subsequently used in Abaqus to perform the static analysis, with the benefit of no additional coordinate systems being defined. The geometric variable, on the other hand, represents a radii ratio (r/R) that relates the inner zone's radius r to the outer zone's radius R in both cases, thus determining the relative size of the two considered regions:

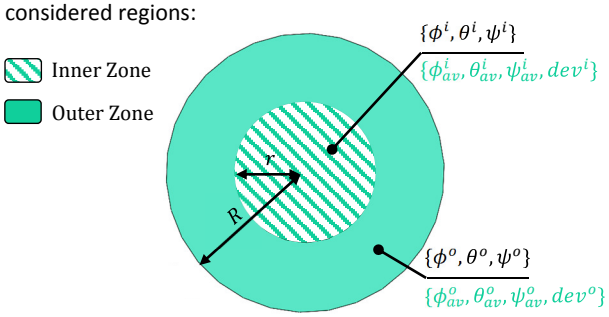

Figure 4 – Schematic of the design variables considered for each material case: single (black) and polycrystal (green).

As for the variables' constraints, the limit values were defined as follows (all angles and deviations in radians):

- $[0, 2\pi]$ for $\phi^i, \phi^o, \psi^i, \psi^o, \phi^i_{av}, \phi^o_{av},, \psi^i_{av}$ and ψ^o_{av};
- $[0, \pi]$ for $\theta^i, \theta^o, \theta^i_{av}$ and θ^o_{av};
- $[0, 5]$ for dev^i and dev^o;
- $[0.05, 0.95]$ for r/R (discrete variable).

Unlike all the other design variables, which are specified as continuous, the radii ratio was only allowed to assume discrete values, spaced out in 0.05 intervals. This is due to the finite element mesh's automatic generation, which was found to be incompatible with certain r/R values.

Lastly, the objective function was defined as:

$$OF(EPOT) = -\sqrt{EPOT^2}\ [V] \quad (13)$$

where $EPOT$ refers to the harvester's electric potential differential, measured in open circuit conditions and in Volts. This variable can be either positive or negative (due to the polarizations' value domain), so, instead of using it directly, transforming this value into its negative absolute allows treating the optimization problem as a minimization, which is the default standard for Matlab´s toolbox optimizers.

4. Computational Model

Every single model created throughout the optimization process needs to be solved. This is achieved through Abaqus, which reads its commands from Python scripts, created iteratively from the design variables' value.

This is the harvester's geometrical setup:

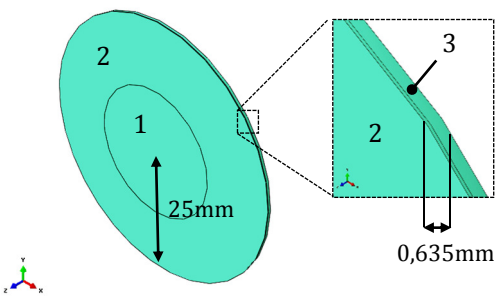

Figure 5 – Harvester geometry and dimensioning: inner (1) and outer (2) piezoelectric layer and substrate layer (3).

Three distinct regions compose this device: two concentric thin PZT-5H piezoelectric layers (0.127 mm thick) overlapped on a thicker aluminum metallic layer (0.508 mm), called substrate. The dimensioning of the circular plate, as well as its boundary conditions and load values, were based on the work of Rupp *et al.* [11].

The following tables contain the considered material properties for all analyses [5,12]:

PZT-5H

Variable [Units]	Value
Elasticity [Pa]	$\begin{bmatrix} 12{,}7 & 8{,}02 & 8{,}47 & & & \\ & 12{,}7 & 8{,}47 & & & \\ & & 11{,}7 & & & \\ & & & 2{,}30 & & \\ & & & & 2{,}30 & \\ & & & & & 2{,}47 \end{bmatrix}_{sim.} \cdot 10^{10}$
Piezoelectric constants (strain form) [m.V^{-1}]	$\begin{bmatrix} & & & & 7{,}41 & \\ & & & 7{,}41 & & \\ -2{,}74 & -2{,}74 & 5{,}93 & & & \end{bmatrix} \cdot 10^{-10}$
Electrical Permittivity [F.m^{-1}]	$\begin{bmatrix} 1{,}51 & & \\ & 1{,}51 & \\ & & 1{,}27 \end{bmatrix}_{sim.} \cdot 10^{-8}$
Density [kg.m^{-3}]	7500

Table 1 – Material properties for PZT-5H. Only non-null matrix entries are shown. All presented matrices are compliant with the IEEE index convention standard.

Aluminum

Variable [Units]	Value
Elasticity [Pa]	$7{,}3 \cdot 10^{10}$
Poisson's Coefficient [ ]	0,33
Density [kg.m^{-3}]	2700

Table 2 – Material properties for aluminum.

The piezoelectric and substrate materials were modelled as anisotropic and isotropic, respectively.

Both electrical and mechanical boundary conditions were applied to the diaphragm: the disk's lateral surface is under an encastre condition, while both the interface and upper surface enforce an electrode condition, where the electric potential remains constant in the latter and null in the former. In addition to these constraints, the device experiences an applied pressure of 9650 Pa on its lower surface.

The elements chosen to model the physical behavior of the device's different regions in Abaqus were the C3D20 and C3D20E. While they are both solid 20 node brick elements, the C3D20E has an additional degree of freedom (besides the ones related to translations) that concerns the electric potential, which is why it is used to model the piezoelectric material.

In order to solve the optimization problem, this finite element model has to be solved iteratively until an optimum solution has been found. This task requires automatizing the harvester's analyses, which was achieved through Matlab coding. The developed program integrates the Abaqus analyses with the optimization algorithms (for the polycrystal case, the homogenization software was also included in this code):

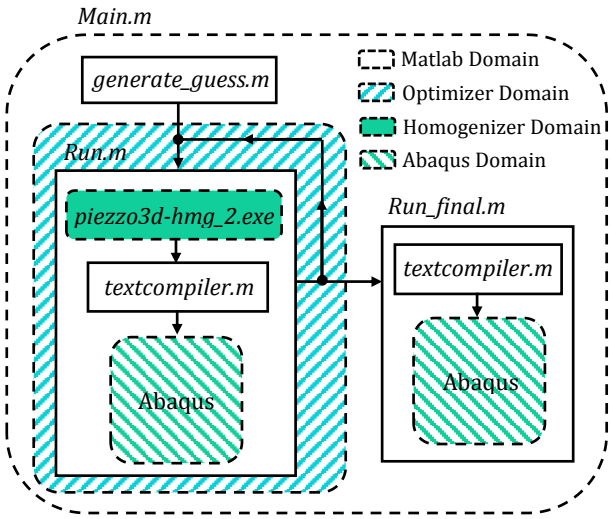

Figure 6 – Simplified schematic of the analyses' automatization, regarding functions and their domains. The homogenizer step is dismissed for the single crystal case.

5. Results

Preliminary adjustments included the mesh refinement study, which determined the discretization level of the analytical finite element model. Once a satisfactory mesh size that was a fair compromise between the solution´s exactness and the simulation time was found, the results from Rupp *et al.* [11] were reproduced. However, both tested Matlab toolbox optimizers had parameters that required tuning.

For the Simulated Annealing algorithm, the most effective cooling schedule was found to be linear. This conclusion was based on nine complete optimizations of the single crystal configuration, three for each considered function. The linear cooling schedule produced the lowest (and therefore best) objective function values, despite a small increase in total execution durations.

A similar study was carried out for the Pattern Search algorithm, regarding the initial size of the optimizer´s search grid or mesh. Although this parameter did not appear to affect the final solution´s value, the total execution time was slightly reduced for an initial mesh size of 1.

5.1 Single Crystal (Case 1)

Based on the outcome of several full optimizations and the tracking of their progression, a maximum number of permitted evaluations to the objective faction was defined as the stopping criterion (400 evaluations for this case).

This strategy allows for the direct comparison between the two tested optimization algorithms and guarantees that a sufficiently optimum solution is always found.

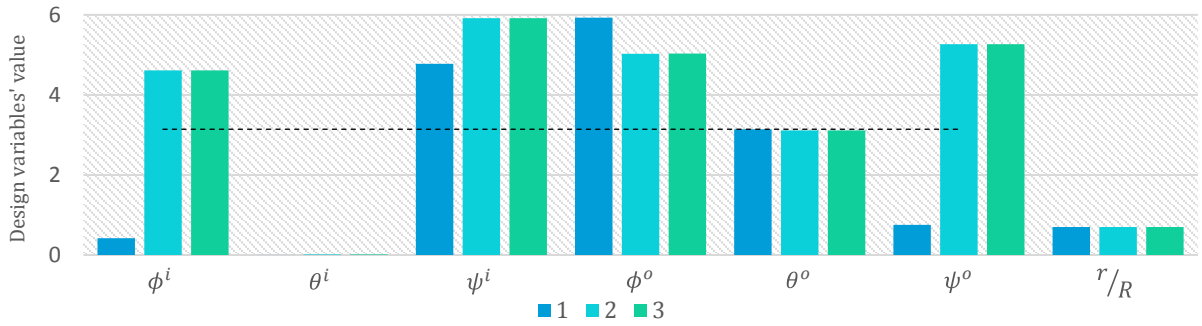

Figure 7 – Design variables' final values, obtained with the SA algorithm on 3 separate executions, for the single crystal case. The dashed line marks π.

The optimized values found for the design variables with the Simulated Annealing (SA) algorithm can be seen in Figure 7 (above). These results were obtained from three separate full optimizations.

The fact that the θ and r/R variables all tend to the same value imply their significance to the electric potential's magnitude. The other angle-related variables (ϕ and ψ) were found to not have any discernible effect on the objective function's value.

These results can be explained through the material's polarization: the θ angle determines the orientation of the main polarization axis, which in turn dictates the preferential direction in which the piezoelectric effect develops. Given that there are two distinct tension states coexisting in the plate (tension and compression) that result from the combined effect of pressure loading and encastre boundary condition, the two independent zones can be optimally excited when their polarization's main axes are opposite and aligned with the loading direction (normal to the plate's surface). Considering the modular value of the output electric potential in the objective function formula also means that θ^i and θ^o can either tend to 0 or π radians.

The optimum ratio that determines the proportion between the inner and outer zones was found to be 0.7, this value being constant in all runs.

The corresponding objective function values can be seen in Figure 8, according to the optimizations' execution order.

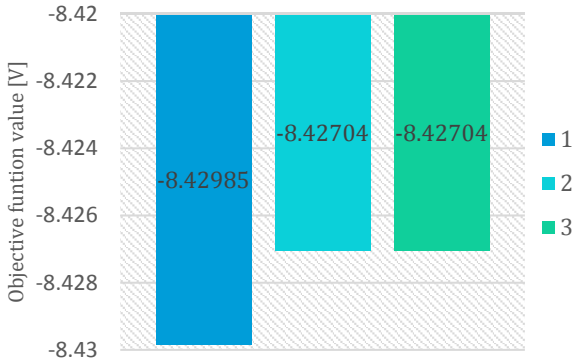

Figure 8 – Optimized objective function values, obtained with the SA algorithm, for the single crystal case.

These results are all in accordance with those determined by Rupp *et al.* [11], having small variance throughout the three separate runs performed.

The results obtained with the Pattern Search (PS) algorithm support those obtained for the SA optimizer. In Figure 9 (below), the design variables' values illustrate the possibility of either θ^i or θ^o tending to 0 or π radians. Again, it is evident that the ϕ and ψ variables hold no apparent influence over the objective function's final value, which is why none of them tend to a concrete value throughout the optimizer's iterations. The optimum radii ratio was also determined to be 0.7, in all three separate runs.

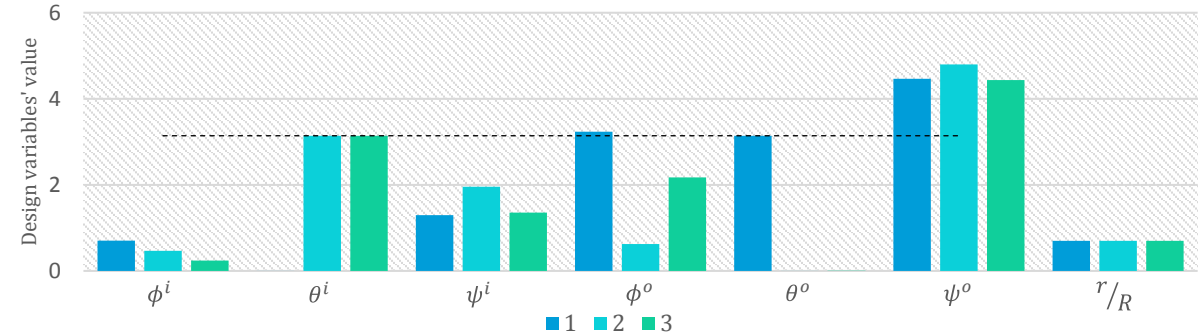

Figure 9 – Design variables' final values, obtained with the PS algorithm on 3 separate executions, for the single crystal case. The dashed line marks π.

Figure 10 resumes the obtained objective function values, for this optimization technique:

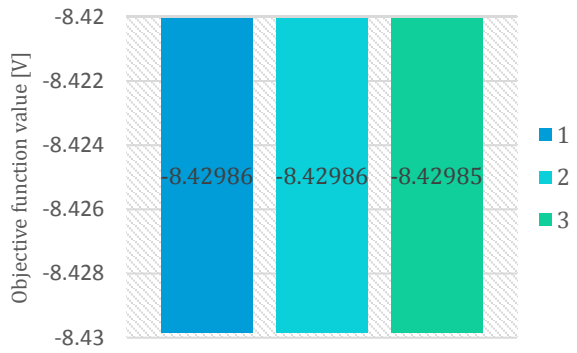

Figure 10 – Optimized objective function values, obtained with the PS algorithm, for the single crystal case.

It is immediately noticeable that these results present a much smaller variability from execution to execution, when compared to the ones obtained through the SA algorithm. The obtained values are nonetheless congruent with the ones presented in Figure 8 for the SA optimizer.

In order to better understand what separates both optimizers, a more comprehensive study was undertaken, so that some mean values could be compared, regarding the final results presented for the single crystal case.

Figures 11, 12 and 13 comprise the results for this study, where the mean values for the objective function, total simulation time and single iteration time are compared for each tested algorithm, respectively.

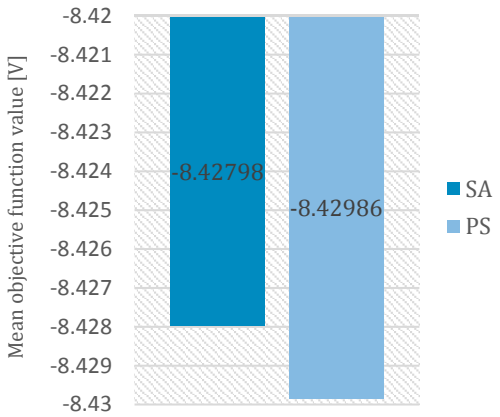

Figure 11 – Comparison between the mean objective function values obtained with the SA and PS algorithms.

Figure 11 shows that the PS algorithm produced the lowest mean objective function value. Both this result and the smaller variability associated with the PS optimizer are a direct consequence of this algorithm's methodical search for the optimal solution.

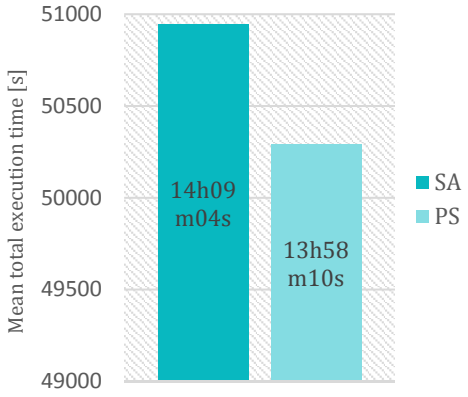

Figure 12 – Comparison between the mean total execution times for the SA and PS algorithms.

In Figure 12, the total execution times point to a slightly lengthier (albeit negligible) operative duration for the SA optimizer.

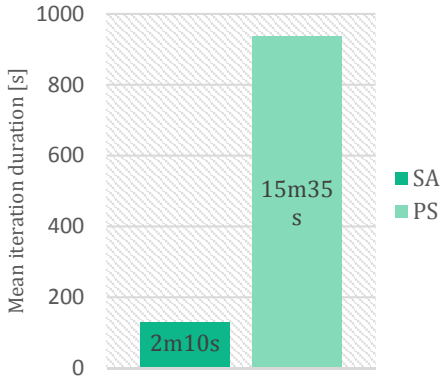

Figure 13 – Comparison between the duration of a single iteration for the SA and PS algorithms.

Figure 13, however, shows a large discrepancy, regarding the duration of a single iteration. In fact, it is important to distinguish the different definitions of 'iteration' that both algorithms imply: the SA optimization technique assumes one objective function evaluation per iteration, since there is no intelligent search or history being kept, whereas with the PS algorithm, the optimizer has to choose a particular search direction at the end of each iteration. To this end, the algorithm must evaluate several harvester configurations (sets of design variables) in different search directions before progressing along any one of them, and so this operation constitutes the definition of an iteration, in this case.

Ultimately, the obtained data supports the claim that, for this particular optimization problem setup, the PS algorithm is better equipped to optimize the harvester structure.

5.2 Polycrystal (Case 2)

The first optimizations performed for this material case revealed that the introduction of statistical variables to treat the piezoelectric medium as polycrystalline did not improve the optimized objective function value, which is to say that, given the choice, the optimization process would always

select the polarization distributions with the lowest associated deviations. This result led to a restructuring of the presentation of results. So, rather than undertaking several pointless optimizations that serve no other purpose than to duplicate and verify the already obtained results in the single crystal case (which they did), a decision was made to study and document the influence of the standard deviation's value effect on the output electric potential measured in the harvester.

Thus, contrary to the high number of optimizations performed for the first material case, a parametric study was conducted, where each data point represents a full optimization operation for a given fixed standard deviation value.

It is relevant to point out that, even though the obtained electric potential is lower in magnitude, this material model describes the properties of piezoelectric ceramics more accurately, given that the process of polling through which these materials gain their polarization are probabilistic, rather than deterministic.

Another aspect that became clear with the first executions of the full code for the polycrystalline material was its greatly increased duration, a direct result of this case's complexity. This increase encouraged the relinquish of one of the optimizers, in order to save on as much computational time as possible. Further testing led to the conclusion that the PS algorithm was the most indicated to solve this optimization problem.

The standard deviations' fixed values were chosen asymmetrically across the defined domain for the variables dev^i and dev^o ($[0,5]$), with a heavier discretization of the interval $[0,2]$. Figure 14 (below) holds the results of the full parametric study for the design variables' values.

Although the graph shown may seem complex and somewhat confusing, there are only three variables that present a consistent behavior along the tested standard deviation values – θ_{av}^i, θ_{av}^o and r/R. Based on the results obtained for the first material case, it was already expected that the significance of these particular variables to the objective function value would continue to outweigh all others. Again, this discrepancy is due to the preponderant role the θ-related variables play in determining the piezoelectric material's main axis of polarization, which explains the apparent randomness of the other polarization variables (ϕ_{av}^i, ϕ_{av}^o, ψ_{av}^i and ψ_{av}^o).

Therefore, the analysis of the graph in Figure 14 will focus primarily on the θ mean angles' and radii ratio's evolution. In order to facilitate the results' interpretation, polarization variables related to a specific rotation angle (ϕ, θ and ψ) are represented with same-shaped symbols.

In the deviations' range of $[0,1]$, the optimized solution still corresponds to the configuration of the harvester where the main polarization axes of the two piezoelectric regions are symmetrically disposed and normal to the plate's surface, i.e., with one having θ_{av} equal to 0 and the other to π. When both polarization distributions have a null standard deviation, the single crystal result is obtained.

Again, since the absolute value of the extracted electric potential was considered, it is the difference between θ_{av}^i and θ_{av}^o that remains relatively constant. Likewise, the optimum radii ratio also holds its value at approximately 0.7, for this range.

This trend in behavior, as far as the polarization variables are concerned, starts to weaken from $dev^i = dev^o = 2$ onward. In this range of the graph ($[2,5]$), the tendency documented thus far dissipates progressively, until the maximum value of the standard deviation is reached ($dev = 5$) and both regions of the device present equal values for θ_{av}. Contrary to the other design variables, the radii ratio shows far lesser variability along the increase in deviation, which implies its significance to the obtained electrical potential. However, when the deviation is at its highest value, this ratio also tends to its maximum value, which is roughly 1. This means that, for a high enough randomness in polarization distribution, the best possible configuration for the harvester will no longer correspond to two independent polarization zones, but only one.

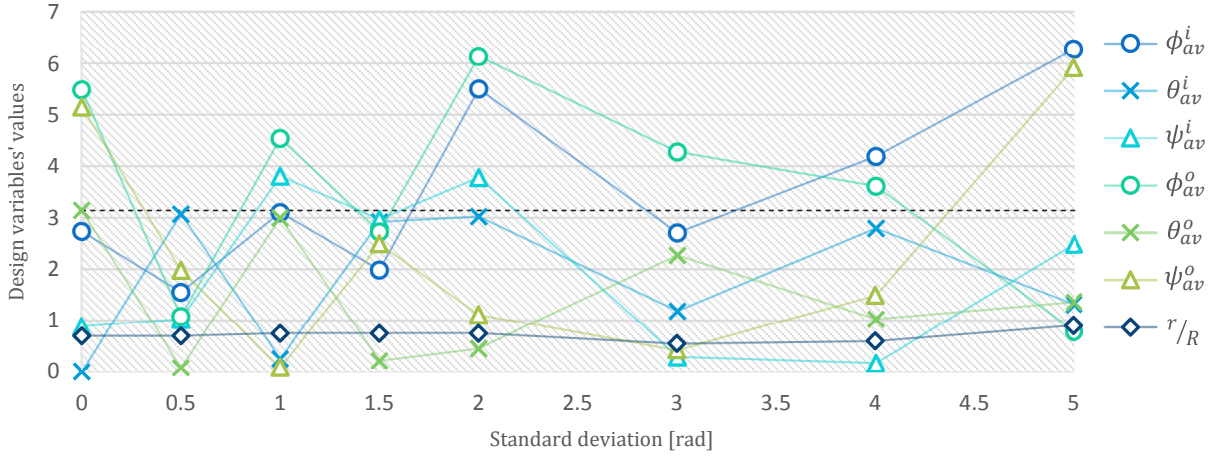

Figure 14 – Optimum value of the design variables as a function of the standard deviations dev^i and dev^o. The dashed line marks π.

Figure 15 presents the objective function value's evolution throughout the different standard deviations tested:

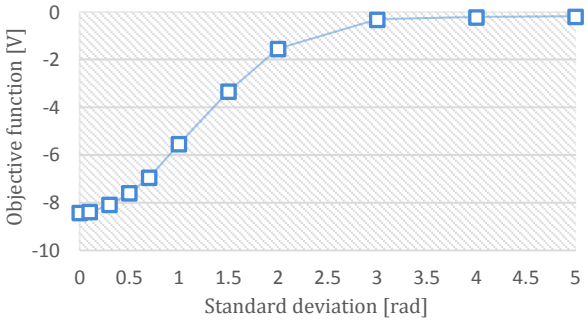

Figure 15 – Objective function value as a function of the standard deviations dev^i and dev^o.

The obtained data points to an increasingly less pronounced piezoelectric effect, which in turn is a direct consequence of the progressive loss of the material properties' directionality. The graph in Figure 15 shows a smooth increase of the electric potential as the standard deviations increase.

For deviations in the range $[0,1]$, the optimized objective function's value starts to slowly rise, until its magnitude drops harshly for the interval $[1,2]$. After this point, it tends asymptotically to zero. The effect of the deviation on the polarization distributions diminishes the piezoelectric effect's strength to such an extent that the design variables lose all their expression in affecting the objective function, thus causing a stagnation in the extracted electric potential.

All the results point to a gradual transition to statistically more disperse material properties, which in turn weaken the piezoelectric effect that the harvester initially displays, until its presence becomes vestigial.

However, it is helpful to point out that a 5 radian standard deviation in a normal distribution comprised between $[0,2\pi]$ (or $[0,\pi]$, for the θ distributions) is less than likely. The ultimate conclusion would be that treating the piezoelectric medium as a polycrystalline material produces reasonably small fluctuations in the extracted electric potential, for a specific interval of deviation values, with the benefit of modelling the material polarizations in a more realistic approach.

6. Conclusions and Future Work

In both studied material cases, an optimization program that can determine the optimum geometric and material characteristics for an open circuit piezoelectric harvester was successfully developed.

In the first case (single crystal), two distinct optimizers were tested and one of them was proven to be more well equipped to solve this specific optimization problem, based on data obtained from executing the developed computational program.

The second case (polycrystalline material) consisted in a parametric study that enabled a better understanding of the influence of the introduction of probabilistic design variables to the harvester model.

Both the single crystal and polycrystal versions of the developed program were constructed in a sufficiently generic and modular way that can accommodate different finite element models. The obtained results encourage the pursuit of the topic of optimization applied to piezoelectric energy harvesting.

Future work may include the testing of different optimization algorithms versus the already obtained data for the Pattern Search optimizer. It would also be of interest to study the applications of different piezoelectric materials with different crystallographic symmetries, some of which (like barium titanate) could improve the output electric potential when subjected to the homogenization process that was applied [6]. The same applies for the number of independent polarization regions considered in the discretization of the piezoelectric layer or even taking in account the stresses in the structure for the optimization process. The main goal would be to develop these optimizations in a closed-circuit condition, although this would be unfeasible to achieve in Abaqus without the implementation of user-defined subroutines that can model electric circuit finite elements.

References

[1] Cochran, S., Nakamura, K. (2012), *Ultrasonic transducers*, Woodhead Publishing.

[2] Vatansever et al. (2012), *Alternative Resources for Renewable Energy: Piezoelectric and Photovoltaic Smart Structures*, in: Singh, B. R., *Global Warming – Impacts and Future Perspective*, InTech, Chapter 10.

[3] Toprak, A., Tigli, O. (2014), *Piezoelectric energy harvesting: State-of-the-art and challenges*, Applied Physics Reviews 1-031104, AIP Publishing.

[4] Yang, J. (2005), *An Introduction to the Theory of Piezoelectricity*, Springer.

[5] Erturk, A., Inman, D. J. (2011), *Piezoelectric Energy Harvesting*, Wiley.

[6] Jayachandran, K. P. *et al* (2009), *Homogenization of textured as well as randomly oriented ferroelectric polycrystals*, Computational Materials Science vol. 45, pp. 816-820, Elsevier B.V.

[7] Lewis, A. (1961), *The Effect of Driving Electrode Shape on the Electrical Properties of Piezoelectric Crystals*, Bell System Tech. J. 40, 1259-1280.

[8] Galka, A. *et al.* (1992), *Homogenization and Thermo-piezoelectricity*, Mechanics Research Communications, Vol. 19, Issue 4, pp. 315-324, Pergamon Press.

[9] Silva, E. C. N. *et al.* (1997), *Optimal design of piezoelectric microstructures*, Computational Mechanics Vol. 19, pp. 397-410, Springer-Verlag.

[10] Arora, J. S. (2004), *Introduction to Optimum Design*, Third Edition, Elsevier.

[11] Rupp, C. J. *et al*. (2009), *Design of Piezoelectric Harvesting Systems: A Topology Optimization Approach Based on Multilayer Plates and Shells*, Journal of Intelligent Material Systems and Structures, Vol. 20, No. 16.

[12] Callister, W. D., Rethwisch, D. G. (2014), *Materials Science and Engineering*, 9th Edition, Wiley.